ARTICLE TEMPLATE

Four-Component Relativistic Density Functional Theory with the Polarizable Continuum Model: Application to EPR Parameters and Paramagnetic NMR Shifts

Roberto Di Remigio[a], Michal Repisky[a*], Stanislav Komorovsky[a], Peter Hrobarik[b], Luca Frediani[a], and Kenneth Ruud[a*]

[a]Centre for Theoretical and Computational Chemistry, Department of Chemistry, University of Tromsø - The Arctic University of Norway, N-9037 Tromsø, Norway
[b]Institut für Chemie, Technische Universität Berlin, Straße des 17. Juni 135, D-10623 Berlin, Germany

ARTICLE HISTORY
Compiled February 24, 2017

ABSTRACT
The description of chemical phenomena in solution is as challenging as it is important for the accurate calculation of molecular properties. Here, we present the implementation of the polarizable continuum model (PCM) in the four-component Dirac–Kohn–Sham density functional theory framework, offering a cost-effective way to concurrently model solvent and relativistic effects. The implementation is based on the matrix representation of the Dirac–Coulomb Hamiltonian in the basis of restricted kinetically balanced Gaussian-type functions, exploiting a non-collinear Kramers unrestricted formalism implemented in the program `ReSpect`, and the integral equation formalism of the PCM (IEF-PCM) available through the standalone library `PCMSolver`. Calculations of EPR parameters ($\boldsymbol{g}$-tensors and hyperfine coupling $\boldsymbol{A}$-tensors), as well as of the temperature-dependent contribution to paramagnetic NMR (pNMR) shifts, are presented to validate the model and to demonstrate the importance of taking both relativistic and solvent effects into account for magnetic properties. As shown for selected Ru and Os complexes, the solvent shifts may amount to as much as 25% of the gas-phase values for $\boldsymbol{g}$-tensor components and even more for pNMR shifts in some extreme cases.

KEYWORDS
relativity; Dirac-Kohn-Sham; EPR; paramagnetic; NMR

1. Introduction

Electron paramagnetic resonance (EPR) spectroscopy [1] is a powerful technique to unravel the structure and spin density of molecules with unpaired electrons. [2, 3] Chemical reactivity is often associated with radical intermediates, and EPR can be used to identify short-lived species in catalytic processes, also in rather complex biological or bioinorganic systems. [4] The analysis of experimental EPR spectra may be difficult, and this process can be substantially facilitated by comparing observed spectra with computed EPR parameters (see *e.g.* Ref. [5]). The EPR parameters most commonly studied using computational methods are the hyperfine coupling (HFC)

*Corresponding authors. Email: michal.repisky@uit.no, kenneth.ruud@uit.no

tensors and the electronic $\boldsymbol{g}$-tensor, which measure the coupling between the effective electron spin of the system and the nuclear magnetic moments or an external magnetic field, respectively. [1] However, other interaction mechanisms can also be observed in the experimental EPR spectra, such as the zero-field splitting (ZFS) due to the interaction between two electron spins in the case of triplet or higher spin multiplicities. [1]

Although the EPR parameters are inherently relativistic in nature, their calculation by means of perturbation theory performs well for molecules with light elements. Studies have been presented both at the level of density-functional theory (DFT), either in a spin-unrestricted [6–11] or a spin-restricted approach [12–14], and at the level of multiconfigurational methods. [15–21] However, for systems with very large relativistic corrections, of which the most important for EPR spectroscopy is the spin–orbit (SO) coupling, the perturbation-based methods fail to reproduce not only the magnitude but also the sign of certain EPR tensor components due to the large sensitivity of these parameters on higher-order SO effects [22–24]. Moreover, the SO coupling may be so strong that there is no longer a direct connection between the spin density and the observed or calculated EPR parameters, mandating an accurate and realistic computational protocol to interpret EPR measurements correctly. Among efficient electronic structure methods capable of predicting EPR parameters for larger systems, for example transition-metal complexes, DFT has already proved its usefulness, in particular when combined with relativistic quantum mechanics based on approximate quasirelativistic (two-component) Hamiltonians or even full (four-component) Dirac Hamiltonian. By this, higher-order spin-orbit relativistic corrections are included from the start in the variational framework. Several two-component DFT implementations have been reported, involving either zeroth-order regular approximation (ZORA) or Douglas–Kroll–Hess (DKH) Hamiltonians. In such studies, spin polarization effects, which are highly relevant for EPR calculations, were either excluded (Kramers-restricted approach) [25–27] or included (Kramers-unrestricted approach) [28–32]. More recently, four-component calculations of EPR parameters became available [24, 33–37], with their clear advantage over two-component methods not only in higher precision but also in the absence of complicated picture-change transformations of magnetic operators. [28–30]

The calculation of paramagnetic nuclear magnetic resonance (pNMR) parameters can be directly related to the parameters of an EPR spin Hamiltonian, as shown for doublet systems by Moon and Patchkovskii [38] and later extended to systems with an arbitrary degeneracy by Van Den Heuvel and Soncini [39]. The recourse to EPR parameters is however not necessary as revealed in a comprehensive pNMR theory by Van Den Heuvel and Soncini [40] and supported by applications to heavy-metal containing systems by Gendron *et al.* [41]. Over time, relativistic effects have been included in the calculation of pNMR parameters of increasing quality: from perturbation corrections [42, 43], via the ZORA Hamiltonian [44] up to the four-component Dirac–Coulomb Hamiltonian [45]. Despite these successes, ZFS effects have only recently been included in the calculation of pNMR shifts for systems with multiplicities higher than a doublet [41, 46, 47], following the theory derived from first principles. [40]

The majority of chemical experiments, including EPR and pNMR spectroscopic measurements, happen in solution or in complex environments [48]. This is challenging for quantum-chemical calculations: to reproduce experimental observations, solvent effects must be included, especially for molecular properties that are sensitive to the environment, such as (p)NMR and EPR parameters [49–52]. However, a full quantum treatment of the solvent is not possible, both because of the large number of solvent molecules that must be included in the solvent model, and because of the dynamics of

the solvent systems. The conceptually simplest approach is to include (parts of) the environment explicitly. [53]. Such *cluster methods* include all relevant intermolecular interactions at the same quantum-chemical level of theory, but it is difficult to achieve convergence with respect to the size of the cluster. Moreover, sampling of the huge conformational space will be computationally expensive and in many cases difficult to achieve.

Focused models offer a practical alternative to include environment effects in quantum-chemical calculations: only a small part of the full system is treated quantum mechanically, whereas the rest is modeled in an approximate way, retaining only the environment effect on the electronic structure of the relevant solvated system. Two main approaches can be identified: quantum mechanics/molecular mechanics (QM/MM) methods [54] and dielectric continuum (DC) methods [55].

In QM/MM methods, both solute and solvent are represented with atomistic details. However, the solute is treated quantum mechanically whereas the solvent molecules are treated with a classical force field [54]. Although the QM/MM methods have received considerable popularity and several works have recently been devoted to QM/MM modeling of electronic $\boldsymbol{g}$-tensors and hyperfine coupling constants of paramagnetic species in solution, [56–61] various questions related to the number of snapshots required to reach convergence of different properties or the size of the solvation shells remain difficult to answer. These aspects have limited the use of the QM/MM methodology as a widespread black-box computational protocol.

In DC models, the solvent molecules are replaced by a structureless continuum characterized by its bulk properties [55, 62]. Continuum models, and the polarizable continuum model (PCM) foremost among these, include only electrostatic solute–solvent interactions in their basic formulations, though other effects can be included. [63, 64] In contrast to the cluster and QM/MM methods, long-range electrostatics and statistical averaging are already included in the continuum formulation. Several applications, combining magnetic properties and the continuum models for the inclusion of solvent effects, have been presented at the non-relativistic or relativistic perturbational level of theory (see, *e.g.* refs. [56, 65, 66], review papers [50–52] and references therein), mostly for organic free radicals because of their ubiquity in biological systems and their relevance as spin probes.

EPR and pNMR spectroscopies are also valuable for compounds containing heavy elements. The importance of relativistic and solvent effects on magnetic resonance parameters is recognized both experimentally and computationally. [51, 67–75] Heavy-element containing compounds are often large, and in order to treat these compounds in solution, the computational protocol must be cost efficient and able to reliably describe both the effects of the environment and relativity. Several groups extensively studied strategies for the calculation of NMR shieldings and nuclear spin–spin couplings using the ZORA or Dirac–Coulomb Hamiltonians. They have used both cluster [68] and cluster/continuum [69, 74, 75] models to describe solvent effects, as well as Born–Oppenheimer molecular dynamics [71, 73] to include additional dynamical effects. All these studies point towards the importance of including at least bulk solvent effects in the computational protocol to achieve agreement with experimentally observed trends.

The main goal of the present work is to bridge the existing gap in computational methodologies and to offer a cost-effective way to concurrently model direct solvent effects and relativistic effects in EPR and pNMR calculations of paramagnetic species. To accomplish this, we extended a recent implementation of the PCM-Self-Consistent Field (SCF) scheme at the relativistic four-component DFT level of theory [76] to the

Kramers-unrestricted regime and assessed the methodology in calculations of EPR $\boldsymbol{g}$- and $\boldsymbol{A}$-tensors, as well as the temperature-dependent contribution to pNMR shifts. The implementation is done in the `ReSpect` [77] program package and utilizes the same modular strategy as exploited in the DIRAC implementation [76]: the PCM functionality is provided by an interface to the independently developed `PCMSolver` library [78].

The rest of the paper is organized as follows. In Section 2 we present the theoretical foundation for our implementation of the PCM model in the calculation of EPR and pNMR parameters at the four-component level of theory. In Section 3 we summarize the computational details, before we present in Section 4 the results of pilot applications. Finally, in Section 5 we give some concluding remarks and an outlook. Note that Hartree atomic units will be used throughout the text.

2. Theory

2.1. *IEF-PCM*

Continuum solvation models are among the simplest focused models for the description of solvent effects [55, 62, 79]. The solvent is replaced by a structureless continuum, described by macroscopic physical properties. The solute is placed in a cavity inside the continuum and the mutual electrostatic polarization of the solute and the solvent is taken into account by means of a continuous electric field, called the *reaction field*, that is modulated by the bulk permittivity of the solvent.

This is a problem of classical electrostatics: given a closed volume V with boundary ∂V inside a dielectric of permittivity ε_r and fully enclosing a charge density ρ_0, find the corresponding electrostatic potential $\psi(\boldsymbol{r})$ in space: [80, 81]

$$\begin{cases} \nabla^2\psi(\boldsymbol{r}) = -4\pi\rho_0(\boldsymbol{r}) \quad \forall \boldsymbol{r} \in V \\ \varepsilon_\mathrm{r}\nabla^2\psi(\boldsymbol{r}) = 0 \quad \forall \boldsymbol{r} \notin V \\ \lim\limits_{|\boldsymbol{r}|\to\partial V^+} \psi(\boldsymbol{r}) = \lim\limits_{|\boldsymbol{r}|\to\partial V^-} \psi(\boldsymbol{r}) \\ \varepsilon_\mathrm{r} \lim\limits_{|\boldsymbol{r}|\to\partial V^+} \dfrac{\partial\psi(\boldsymbol{r})}{\partial\hat{\boldsymbol{n}}} = \lim\limits_{|\boldsymbol{r}|\to\partial V^-} \dfrac{\partial\psi(\boldsymbol{r})}{\partial\hat{\boldsymbol{n}}} \end{cases} \tag{1}$$

The first and second partial differential equations (PDEs) are augmented by the last two equations that impose the proper boundary conditions. We require that $\psi(\boldsymbol{r})$ is continuous across the cavity boundary and that its directional derivative have a finite jump, related to the permittivity constant ε_r, across the cavity boundary. The directional derivatives are taken with respect to the surface normal vector $\hat{\boldsymbol{n}}$, from the inside (subscript $+$) and from the outside (subscript $-$) relative to the cavity boundary.

In the integral equation formalism (IEF) of the PCM [82], the system in Eq. (1) is recast as an integral equation [83, 84] whose domain is the surface of the cavity boundary ∂V, a 2-manifold. We represent the electrostatic potential as

$$\psi(\boldsymbol{r}) = \int_V \mathrm{d}^3\boldsymbol{r}' \frac{\rho_0(\boldsymbol{r}')}{|\boldsymbol{r}-\boldsymbol{r}'|} + \int_{\partial V} \mathrm{d}\boldsymbol{t} \frac{\sigma(\boldsymbol{t})}{|\boldsymbol{r}-\boldsymbol{t}|} = \varphi + \xi, \tag{2}$$

where φ is the Newton potential, i. e. the Molecular Electrostatic Potential (MEP)

generated by ρ_0 *in vacuo*. The second term is the *reaction field* and is parametrized in terms of the Apparent Surface Charge (ASC) $\sigma(\boldsymbol{t})$, a charge distribution spread over the cavity boundary. It can be shown that the ASC is the unique solution to the integral equation [82]

$$\left[2\pi\left(\frac{\varepsilon_\mathrm{r}+1}{\varepsilon_\mathrm{r}-1}\right)\hat{\mathcal{I}}-\hat{\mathcal{D}}\right]\hat{\mathcal{S}}\sigma=-\left(2\pi\hat{\mathcal{I}}-\hat{\mathcal{D}}\right)\varphi, \tag{3}$$

where the integral operators are expressed by means of the Green's function for the differential operator in Eq. (1):

$$\begin{aligned}(\hat{\mathcal{S}}f)(\boldsymbol{t}) &= \int_{\partial V}\mathrm{d}\boldsymbol{t}' G(\boldsymbol{t},\boldsymbol{t}')f(\boldsymbol{t}'),\\ (\hat{\mathcal{D}}f)(\boldsymbol{t}) &= \int_{\partial V}\mathrm{d}\boldsymbol{t}'[\nabla_{\boldsymbol{t}'}G(\boldsymbol{t},\boldsymbol{t}')f(\boldsymbol{t}')]\cdot\hat{\boldsymbol{n}}_{\boldsymbol{t}'},\\ G(\boldsymbol{r},\boldsymbol{r}') &= \frac{1}{|\boldsymbol{r}-\boldsymbol{r}'|}\end{aligned} \tag{4}$$

with $\hat{\mathcal{I}}$ being the identity operator. The ASC fully determines the reaction field and the mutual polarization between the solute and the solvent. Furthermore, the full three-dimensional problem in Eq. (1) has been reduced to the determination of a scalar function of the surface coordinate $\boldsymbol{t}$. The integral equation formalism is also quite general: knowledge of the boundary conditions and the Green's function for any linear, elliptic PDE is sufficient in order to set up the associated integral equation. IEF-PCM is not restricted to homogeneous, uniform dielectrics, and extensions have been presented for ionic liquids and liquid crystals [82], dielectric interfaces [85, 86] and metal nanoparticles [87].

The Boundary Element Method (BEM) is the standard method to solve integral equations such as the IEF-PCM equation Eq. (3). The surface of the molecular cavity is discretized into finite elements with a basis set of piecewise regular functions attached [88]. It is then possible to discretize the integral operators $\hat{\mathcal{S}}$ and $\hat{\mathcal{D}}$, the unknown ASC σ and the MEP φ. This leads to a linear system of equations [83]. In our implementation, [78] we use the GePol algorithm to discretize the cavity boundary. In this approach, [89] the cavity is defined as a set of interlocking spheres which are divided into N_ts spherical triangles Δ_i by means of an equilateral partitioning algorithm. We apply a parametrized, one-point, collocation scheme [55, 90] to obtain the linear system of equations. The centroids of the spherical triangles are chosen as collocation points. Eventually, the linear equations are solved by direct LU decomposition. Detailed expressions for the matrix elements of the discretized boundary integral operators can be found in Refs. [55, 90].

We note at this point that the conductor-like screening model (COSMO) [91–93] is a special case of Eq. (3), and the COSMO equation [93]

$$\hat{\mathcal{S}}\sigma=-f(\varepsilon_\mathrm{r})\varphi, \tag{5}$$

can be obtained by taking the infinite-permittivity limit of Eq. (3), or starting from Eq. (1) and assuming conductor-like boundary conditions. The correction factor $f(\varepsilon_\mathrm{r})=\frac{\varepsilon_\mathrm{r}-1}{\varepsilon_\mathrm{r}+X}$ $(0\leq X\leq 1)$ is added to account for the fact that the solvent is a dielectric medium rather than a proper conductor.

2.2. *Four-component EPR theory*

The theoretical foundations for the calculation of the EPR $\boldsymbol{g}$-tensor and hyperfine coupling $\boldsymbol{A}$-tensor in the framework of four-component Dirac–Kohn–Sham (DKS) theory have been described previously [35, 36]. Here we will only briefly recapitulate the details of the implementation in the `ReSpect` program package [77]. In the following, we will assume summation over repeated indices and adopt the following notation: the indices λ, τ, μ, ν will denote atomic orbitals (AO), u, v will denote Cartesian components of tensors and i will be used as index for occupied molecular orbitals (MO).

The EPR $\boldsymbol{g}$- and $\boldsymbol{A}$-tensors are calculated in four-component theory as first-order molecular properties, which is equivalent for variational methods such as DKS to the calculation of an expectation value by virtue of the Hellmann-Feynman theorem [94]

$$g_{uv} = \frac{2c}{\langle \tilde{S}_v \rangle} \operatorname{Tr}\left\{ \boldsymbol{\Lambda}_{B_u} \boldsymbol{D}^{(J_v)} \right\}, \tag{6}$$

$$A^M_{uv} = \frac{1}{\langle \tilde{S}_v \rangle} \operatorname{Tr}\left\{ \boldsymbol{\Lambda}_{I^M_u} \boldsymbol{D}^{(J_v)} \right\}. \tag{7}$$

Here, c is the speed of light and $\langle \tilde{S}_v \rangle$ is an effective spin of the system. The matrices with elements $\boldsymbol{\Lambda}_{\lambda\tau}$ are the four-component representation of the perturbation operators in a restricted kinetically balanced (RKB) basis set:

$$(\boldsymbol{\Lambda}_{B_u})_{\lambda\tau} = \frac{1}{2} \left\langle \boldsymbol{X}_\lambda \left| \left(\boldsymbol{r}_G \times \boldsymbol{\alpha} \right)_u \right| \boldsymbol{X}_\tau \right\rangle, \tag{8}$$

$$\left(\boldsymbol{\Lambda}^{\mathrm{PN}}_{I^M_u}\right)_{\lambda\tau} = \gamma^M \left\langle \boldsymbol{X}_\lambda \left| \left(\frac{\boldsymbol{r}_M \times \boldsymbol{\alpha}}{r_M^3} \right)_u \right| \boldsymbol{X}_\tau \right\rangle, \tag{9}$$

$$\left(\boldsymbol{\Lambda}^{\mathrm{FN}}_{I^M_u}\right)_{\lambda\tau} = \gamma^M \left\langle \boldsymbol{X}_\lambda \left| \left[\boldsymbol{\alpha} \times \boldsymbol{\nabla} \int \left(\frac{\eta}{\pi}\right)^{3/2} \frac{\mathrm{e}^{-\eta(\boldsymbol{R}-\boldsymbol{R}_M)^2}}{|\boldsymbol{r}-\boldsymbol{R}|} \, \mathrm{d}^3\boldsymbol{R} \right]_u \right| \boldsymbol{X}_\tau \right\rangle, \tag{10}$$

$\boldsymbol{r}_M$ ($\boldsymbol{r}_G$) is the electron position vector $\boldsymbol{r}$ relative to the coordinates of the Mth nucleus $\boldsymbol{R}_M$ (gauge origin $\boldsymbol{R}_G$). The Dirac matrices $\boldsymbol{\alpha}$ and β are composed of the two-by-two zero (0_2), unit (1_2), and Pauli spin matrices $\boldsymbol{\sigma} = (\sigma_x, \sigma_y, \sigma_z)$

$$\boldsymbol{\alpha} = \begin{pmatrix} 0_2 & \boldsymbol{\sigma} \\ \boldsymbol{\sigma} & 0_2 \end{pmatrix}, \qquad \boldsymbol{\beta} = \begin{pmatrix} 1_2 & 0_2 \\ 0_2 & -1_2 \end{pmatrix}. \tag{11}$$

Although we provide expressions for both point nucleus (PN) Eq. (9) and finite nucleus (FN) Eq. (10) models of the magnetic moment distribution, in the present work the PN model was used only. The effects of these two models in the four-component calculations of the $\boldsymbol{A}$-tensor have been discussed in Ref. [36]. The RKB basis has the four-by-four matrix form

$$\boldsymbol{X}_\lambda = \begin{pmatrix} 1_2 & 0_2 \\ 0_2 & \frac{1}{2c}\boldsymbol{\sigma}\cdot\boldsymbol{p} \end{pmatrix} \chi_\lambda, \tag{12}$$

with χ_λ representing a Gaussian-type scalar function, $\boldsymbol{\sigma}$ is the vector composed of Pauli matrices, and $\boldsymbol{p}$ is the momentum operator.

The one-particle density matrix in Eqs. (6) and (7) is defined as

$$\boldsymbol{D}^{(J_v)}_{\lambda\tau} = \boldsymbol{C}^{(J_v)}_{\lambda i}\boldsymbol{C}^{(J_v)\dagger}_{\tau i}, \tag{13}$$

where the occupied molecular orbital coefficients $\boldsymbol{C}_{\lambda i}$ are obtained from the four-component analogue of the Roothaan–Hall equations

$$\boldsymbol{F}^{(J_v)}\boldsymbol{C}^{(J_v)} = \boldsymbol{S}\boldsymbol{C}^{(J_v)}\boldsymbol{\epsilon}^{(J_v)}, \tag{14}$$

where $\boldsymbol{S}$ is the overlap matrix, defined as

$$\boldsymbol{S}_{\lambda\tau} = \langle \boldsymbol{X}_\lambda \,|\, \boldsymbol{X}_\tau \rangle\,, \tag{15}$$

and $\boldsymbol{\epsilon}^{(J_v)}$ the orbital (one-electron) energies [95, 96].

The superscript (J_v) indicates the dependence of the molecular orbitals on the orientation of the magnetization vector $\boldsymbol{J}$. If the magnetization vector is oriented along the principal axes of the $\boldsymbol{g}$-tensor, the calculation of the $\boldsymbol{g}$- and $\boldsymbol{A}$-tensors will only require three solutions of the Kramers unrestricted Roothaan–Hall equations Eq. (14). From each solution, one diagonal component of the $\boldsymbol{g}$-tensor and one column of the $\boldsymbol{A}$-tensor is obtained. However, this approach requires that the principal axes of the $\boldsymbol{g}$-tensor are known prior to the calculations. In case of systems with high symmetry, such as the $[\mathrm{ReNX}_n]^-$ complexes studied in this work, the orientation of the $\boldsymbol{g}$-tensor principal axes is known *a priori* and coincides with symmetry axes. In more general cases, results from preliminary one-component perturbation calculations can be used as starting guess. Subsequently, a series of four-component calculations are carried out and after each calculation the $\boldsymbol{g}$-tensor is rotated and new principal axes are determined. The orientation of the principal axes is usually converged within a single iteration. For a more detailed discussion of four-component $\boldsymbol{g}$-tensor calculations and the differences between Kramers restricted and unrestricted methods can be found in Refs. [35, 97].

In the following we will omit the (J_v) superscript to simplify the notation. The Dirac–Hartree–Fock (DHF, $\theta = 1$) or Dirac–Kohn–Sham ($0 \leq \theta < 1$) vacuum Fock matrix can be divided into one- and two-electron contributions:

$$\boldsymbol{F}_{\mathrm{vac}} = \boldsymbol{h}^{\mathrm{D}} + \boldsymbol{G}[\theta, \boldsymbol{D}] + \boldsymbol{V}^{\mathrm{xc}}[(1-\theta), \boldsymbol{D}]. \tag{16}$$

$\boldsymbol{h}^{\mathrm{D}}$ represents the one-electron Dirac Hamiltonian in the RKB basis

$$\boldsymbol{h}^{\mathrm{D}}_{\lambda\tau} = \left\langle \boldsymbol{X}_\lambda \,\middle|\, c\boldsymbol{\alpha}\cdot\boldsymbol{p} + (\beta - 1_4)c^2 + V^{\mathrm{nuc}}1_4 \,\middle|\, \boldsymbol{X}_\tau \right\rangle, \tag{17}$$

with $\boldsymbol{\alpha}$ and β matrices defined by Eqs. (11), and the scalar nuclear–electron attraction potential operator

$$V^{\mathrm{nuc}} = -\sum_M Z_M \int \left(\frac{\eta}{\pi}\right)^{3/2} \frac{\mathrm{e}^{-\eta(\boldsymbol{R}-\boldsymbol{R}_M)^2}}{|\boldsymbol{r}-\boldsymbol{R}|}\,\mathrm{d}^3\boldsymbol{R}, \tag{18}$$

and Z_M the nuclear charge. Here, we have assumed a finite-sized nuclear model of Gaussian type where both the nuclear charge and magnetic moment distributions are modelled with the same s-type Gaussian function. This approximation is justified

because the $\boldsymbol{A}$-tensor is only weakly dependent on the particular finite magnetic moment distribution. [98] The two-electron contribution $\boldsymbol{G}$ describes the instantaneous Coulomb electron-electron interaction. It consists of a Coulomb ($\boldsymbol{J}$) and an exchange part ($\boldsymbol{K}$)

$$\boldsymbol{G}[\theta] = \boldsymbol{J} - \theta\boldsymbol{K}, \tag{19}$$

$$\boldsymbol{J}_{\lambda\tau} = \iint \frac{\boldsymbol{\Omega}_{\lambda\tau}(\boldsymbol{r})\boldsymbol{D}_{\mu\nu}\boldsymbol{\Omega}_{\nu\mu}(\boldsymbol{r}')}{|\boldsymbol{r}-\boldsymbol{r}'|}\,\mathrm{d}^3\boldsymbol{r}\,\mathrm{d}^3\boldsymbol{r}', \tag{20}$$

$$\boldsymbol{K}_{\lambda\tau} = \iint \frac{\boldsymbol{\Omega}_{\lambda\mu}(\boldsymbol{r})\boldsymbol{D}_{\mu\nu}\boldsymbol{\Omega}_{\nu\tau}(\boldsymbol{r}')}{|\boldsymbol{r}-\boldsymbol{r}'|}\,\mathrm{d}^3\boldsymbol{r}\,\mathrm{d}^3\boldsymbol{r}', \tag{21}$$

where $\boldsymbol{r}$ and $\boldsymbol{r}'$ are variables in $\mathbb{R}^3$, and $\boldsymbol{\Omega}_{\lambda\tau} = \boldsymbol{X}_\lambda^\dagger \boldsymbol{X}_\tau$ is the overlap distribution of two four-component basis functions, as defined in Eq. (12). Note that the order of the four-by-four matrices in the numerator of Eq. (21) is fixed, since they do not commute.

The construction of the Fock matrix Eq. (16) requires the non-collinear exchange-correlation (XC) potential for generalized-gradient approximation (GGA) functionals. In our implementation, we use the following definition of the non-collinear XC potential

$$\begin{aligned}\boldsymbol{V}_{\lambda\tau}^{\mathrm{xc}} = \int \Bigg(&\frac{\partial\epsilon^{\mathrm{xc}}}{\partial n}\boldsymbol{\Omega}_{\lambda\tau} + \frac{\partial\epsilon^{\mathrm{xc}}}{\partial s}\frac{\rho_k}{s}\boldsymbol{\Omega}_{\lambda\tau}^k \\ &+ \frac{\partial\epsilon^{\mathrm{xc}}}{\partial(\nabla_l n)}\nabla_l\boldsymbol{\Omega}_{\lambda\tau} + \frac{\partial\epsilon^{\mathrm{xc}}}{\partial(\nabla_l s)}\frac{\rho_k}{s}\nabla_l\boldsymbol{\Omega}_{\lambda\tau}^k\Bigg)\,\mathrm{d}^3\boldsymbol{r},\end{aligned} \tag{22}$$

where ϵ^{xc} denotes the XC energy density, which depends on the electron charge density n and the length of the electron spin density vector s

$$n = \mathrm{Tr}\left[\boldsymbol{D}\boldsymbol{\Omega}\right], \qquad s = \sqrt{\rho_x^2 + \rho_y^2 + \rho_z^2}, \qquad \rho_k = \mathrm{Tr}\left[\boldsymbol{D}\boldsymbol{\Omega}^k\right], \tag{23}$$

$$\boldsymbol{\Omega}_{\lambda\tau}^k = \boldsymbol{X}_\lambda^\dagger \boldsymbol{\Sigma}_k \boldsymbol{X}_\tau, \qquad \boldsymbol{\Sigma}_k = \begin{pmatrix}\sigma_k & 0_2 \\ 0_2 & \sigma_k\end{pmatrix}, \tag{24}$$

with $\boldsymbol{\Sigma}_k$ being the four-component spin operator. Since we consider here only systems with a degenerate ground state, both the spin density and its gradient are nonzero, in contrast to systems with a nondegenerate ground state. The form of the non-collinear XC potential for local density approximation (LDA) functionals, given by the first two terms on the right-hand side of Eq. (22), has previously been presented by Sandratskii [99] and van Wüllen [100]. A straightforward extension of these LDA expressions to nonzero gradients of the spin density suffers from numerical instabilities as discussed by Scalmani and Frisch [101]. The expression in Eq. (22) is both numerically stable and includes gradients of the spin density in a non-collinear fashion. The physical motivation for the definition in Eq. (22), as well as a discussion of numerical instabilities, will be presented elsewhere.

The final ingredient in the construction of the Fock matrix in Eq. (14) is the additional one-electron PCM potential. Detailed derivations have already been given, both in the context of one-component [55, 79] and four-component methods [76]. The vacuum Fock matrix in Eq. (16) is augmented by the PCM one-electron potential

$$\boldsymbol{F} = \boldsymbol{F}_{\mathrm{vac}} + \boldsymbol{V}^{\mathrm{PCM}}, \tag{25}$$

with

$$\boldsymbol{V}^{\mathrm{PCM}} = \int_{\partial V} \sigma(\boldsymbol{t})\boldsymbol{\varphi}(\boldsymbol{t})\,\mathrm{d}\boldsymbol{t}. \tag{26}$$

Note that in the previous equation, σ is *not* a Pauli matrix but rather the ASC as computed by solving Eq. (3). The representation of the MEP operator in a four-component RKB basis is given by

$$\boldsymbol{\varphi}_{\lambda\tau}(\boldsymbol{t}) = -\int \frac{\boldsymbol{\Omega}_{\lambda\tau}(\boldsymbol{r})}{|\boldsymbol{r}-\boldsymbol{t}|}\,\mathrm{d}^3\boldsymbol{r}. \tag{27}$$

Note that only the large–large and small–small component blocks remain nonzero because the Coulomb interaction is represented by a scalar multiplicative operator. In Eq. (25), we use the nondiscretized form of the PCM Fock matrix contribution, in contrast to the form presented in Ref. [76]. The two forms are equivalent, but the current formalism is more general as it does not require either a reference to the PCM model adopted (IEF-PCM or COSMO) or the use of a BEM scheme to solve the classical PCM problem.

2.3. *Four-component pNMR theory*

The NMR chemical shift of paramagnetic substances is in general temperature-dependent and it is therefore customary to decompose the total isotropic pNMR shift into two contributions

$$\delta_M = \delta_M^{\mathrm{orb}} + \delta_M^{\mathrm{para}} \tag{28}$$

The orbital contribution δ_M^{orb} is approximately temperature-independent (neglecting the rovibrational motion of the nuclei), in contrast to the paramagnetic contribution δ_M^{para} which usually exhibits a strong temperature-dependence [102–104]. These contributions can be separated in experimental measurements by plotting the temperature dependence of the pNMR signals against $1/T$, where the slope and the intercept with the vertical axis are related to the paramagnetic and orbital contributions to the pNMR shifts, respectively. In this work we exclusively focus on the paramagnetic contribution to the pNMR shift, which for systems with a doubly degenerate ground state has the form (see Refs. [38, 42])

$$\delta_M^{\mathrm{para}} = \frac{\mu_e}{12\gamma^M kT}\,\mathrm{Tr}\left(\boldsymbol{g}\boldsymbol{A}_M^{\mathrm{T}}\right) \tag{29}$$

Here μ_e is the Bohr magneton, kT is the thermal energy, and $\boldsymbol{g}$ and $\boldsymbol{A}_M$ are corresponding EPR tensors as defined in Eqs. (6) and (7). From Eq. (29) it follows that accurate measurements of the paramagnetic shift provide us with an indirect link to the EPR parameters. This connection has already been examined in the framework of relativistic four-component DFT theory [45].

3. Computational details

Structures of the small Re^{VI} compounds and larger *trans*- $[Ru^{III}Cl_4(DMSO)(4\text{-R-py})]^-$ complexes were taken from the Supporting Information of Ref. [24] and Ref. [67], respectively. Structures of the Ru and Os nitrosyl complexes were optimized in the `Turbomole` program using the PBE0 [105, 106] hybrid functional with Grimme's atom-pairwise D3 dispersion corrections [107] and Becke–Johnson (BJ) damping [108]. Quasirelativistic energy-consistent, small-core pseudopotentials (effective-core potentials, ECP) [109] were used for the metal centers, with (7s7p5d1f)/ [6s4p3d1f] and (8s7p6d1f)/[6s4p3d1f] Gaussian-type orbital valence basis sets for the 4d and 5d metal atoms, respectively. Ligand atoms were treated with an all-electron def2-TZVP basis set [110]. All the geometries are collected in the Supporting Information. The property calculations were carried out at the four-component DKS level of theory with the developers version (3.5.0) of the relativistic quantum chemistry program `ReSpect`. [77] The hybrid PBE0 functional and its modified form with a customized admixture of 40% Hartree–Fock exchange (PBE0-40) were used, respectively. In our previous studies, the PBE0-40 functional was found to provide good agreement with experimental data, clearly outperforming generalized-gradient approximation (GGA) functionals, in particular for the hyperfine couplings. [24] The exchange–correlation contribution was evaluated numerically on an integration grid consisting of 80 radial grid points and a Lebedev angular grid with an adaptive size and its rotationally invariant implementation was preserved by means of a non-collinear approach with the spin density described as the norm of the spin magnetization vector (see Section 2.2). For all nuclei, a finite-sized Gaussian distribution model for the nuclear charge was applied with parameters taken from Ref. [111], whereas a simple point model was used for nuclear magnetic moments. To represent the large-component spinors, all-electron Gaussian-type basis sets of polarized triple-zeta quality were used: the uncontracted form of Jensen's pcJ-2 basis for elements of the first three periods (upcJ-2) [112], and the uncontracted form of Dyall's vTZ basis set [113–115] for the heavy elements. A restricted kinetic balance condition was imposed at the integral level to construct the small-component basis. The evaluation of the two-electron contributions to the Fock matrix is the dominant computational task, especially in four-component-based methodologies. To reduce the cost of this essential step, an *atom-pair approximation* for the electron repulsion integrals was used: the evaluation of four-center two-electron integrals over atom-centered small-component basis functions χ^S is discarded, unless the bra and ket basis pairs share the same origin, *i.e.* $[\chi^S_A\chi^S_B|\chi^S_C\chi^S_D]\delta_{AB}\delta_{CD}$, where δ is the Kronecker delta and A, B, C, and D refer to the origin of the basis functions. Unless stated otherwise, the cavities used for the PCM were generated using van der Waals radii from Allinger's MM3 model [116]: 1.62 Å for H, 2.04 Å for C, 1.93 Å for N. 1.82 Å for O, 1.71 Å for F, 2.15 Å for S, 2.07 Å for Cl, 2.34 Å for Ru, 2.37 Å for Re, and 2.35 Å for Os, all scaled down by a factor of 1.2. The addition of spheres not centered on the nuclei was disabled and a tesselation with an average finite element area of 0.3 $Å^2$ was used.

4. Applications

In this study, we will only be concerned with the so-called *direct* solvent effects—that is, solvent effects arising directly from the mutual polarization of the solvent and the solute density. *Indirect solvent effects* arising from the relaxation of the molecu-

lar structure upon solvation are not considered here. This setup enables to ease the interpretation of the results, as they only contain direct solvent effects.

Initial validation studies of our 4c-mDKS/IEF-PCM implementation on a series of $[MEX_n]^q$ d^1 complexes, investigated previously using various relativistic approaches *in vacuo*, [24] revealed a minor effect of the continuum solvent model on the EPR parameters. The results for selected Re^{VI} complexes, $[ReNF_4]^-$ and $[ReNCl_4]^-$, in the gas-phase and in CH_3CN solution are presented in Table 1. The solvent shifts (the differences between EPR parameters computed with and without inclusion of the PCM solvent model) amount to only a few ppt for Δg-tensor components (with a maximum of -9 ppt for $\Delta g_{\|}$ in $[ReNF_4]^-$) and up to 40-50 MHz for metal hyperfine coupling (HFC) constants. Although these solvent shifts should be considered in highly accurate EPR calculations, they are smaller or comparable to the experimental error and much less pronounced than the effect of DFT functional and/or basis set, see Table 1 and corresponding footnotes. Comparably small solvent shifts are also found for other members of the $[MEX_n]^q$ benchmark series. Our previous conclusion on the "best performing" hybrid DFT functionals (with an optimal Hartree–Fock exchange admixture of about 25–40% for $\boldsymbol{g}$-tensors and 40% for HFCs) for selected d^1 compounds remains valid and virtually unaffected by the inclusion of direct solvent effects. [24]

In contrast, we found a notable effect of the solvent polarity on electronic $\boldsymbol{g}$-tensor components within a series of low-spin Ru and Os complexes (see Figure 1 for the structures). The results computed *in vacuo* and using the PCM solvent model for selected nitrosyl complexes, characterized experimentally by EPR spectroscopy in highly polar acetonitrile frozen solutions, are presented in Table 2. It is obvious that both relativistic and matrix effects are required to reproduce the experimental values in these systems. In general, solvent shifts of several tens ppt are observed for the Δg_{11} component and amount up to 109 ppt in $[Os(CN)_5(NO)]^{3-}$ at the PBE0-40 level. Such a solvent shift corresponds to ca. a 25% contribution to the overall g_{11} value and it is larger than the effect of Hartree–Fock exchange admixture or the variation of the Δg_{11} values in Ru nitrosyl complexes upon ligand substitution[117]. Note that the Δg_{11} axis lies in the M-N-O plane and it is nearly parallel to the N-O bond; cf. Figure 2a. A smaller, but still remarkable, solvent effect is also noticed for Δg_{22} and Δg_{iso} values in Os complexes. Interestingly, the solvent effect on Δg_{11} and Δg_{22} in anionic $[M(CN)_5(NO)]^{3-}$ species have positive values, while they are negative in cationic $[MCl(bpy)_2(NO)]^+$ complexes. Nevertheless, the use of the PCM model improves the agreement of computed $\boldsymbol{g}$-tensor shifts with experimental data in both cases and demonstrates the sensitivity of EPR parameters to solvent polarity in these systems, see Table 2 and Figure 2.

We note in passing, that sizeable solvent effects on electronic $\boldsymbol{g}$-tensor and metal HFCs were found, *e.g.* for some Cu(II) complexes, but these were primarily caused by the change of the metal coordination environment (upon solvent coordination or protonation of ligands) rather than by solvent polarity alone, as also confirmed by DFT calculations. Here, the PCM model is not sufficient to reproduce the observed trends and explicit solvent molecules have to be considered in the calculations. [118–120]

Due to the lack of experimental data on HFCs in the investigated nitrosyl complexes, benchmark studies were also performed for the temperature-dependent part of pNMR shifts, which are for doublets inherently associated with the product of the electronic $\boldsymbol{g}$-tensor and HFC tensor of the nucleus in question, see Eq. (29). As model systems, we selected two Ru(III) low-spin d^5 complexes (S=1/2) studied comprehensively for their ^1H and ^{13}C NMR shifts in highly polar dimethylformamide (DMF) as a function of temperature. [67] Experimental temperature-dependent pNMR shifts

along with computed data *in vacuo* and in solution are collected in Table 3. A significant improvement of the computed pNMR shifts upon inclusion of bulk solvent effects can be noticed; the mean-absolute error (MAE) is reduced from 10-20 ppm to about 2-4 ppm. These MAE are compararable to or slightly better than errors obtained by using the COSMO solvation model in conjunction with the two-component ZORA-SO Hamiltonian, implemented in the ADF software package. Closer inspection (see Tables 1 and 2 in Supporting Information) revealed that these solvent shifts are governed by changes in both the electronic $\boldsymbol{g}$-tensor and HFC tensors of the ligand atoms, the latter being more dominant. HFCs are affected more by solvent polarity than the $\boldsymbol{g}$-tensor components in relative terms; e.g. the solvent shifts are about 5% for g_{iso}, whereas they contribute more than 50% to A_{iso} in some cases. Interestingly, apart from changing the magnitude of the pNMR shifts, bulk solvent effects may also invert their sign due to a change of the spin density distribution in response to the solvent polarity, as demonstrated e.g. for C3 in the 4-CN-substituted pyridine complex.

Finally, we note that the choice of atomic van der Waals radii used in the construction of the molecular solvent-accessible surface can have a substantial impact on the calculated results. In the systems studied, using the universal force field-derived (UFF) radii [121] provides results that do not compare to experiments as well as when using the radii derived from Allinger's MM3 model [116].

5. Summary

We have presented an extension of the polarizable continuum model for solvation to the calculation of EPR $\boldsymbol{g}$-tensors and hyperfine coupling constants as well as the temperature dependent contribution to paramagnetic NMR chemical shifts at the relativistic four-component density-functional theory level. The small component basis set is generated at the integral level by imposing the restricted kinetic balance condition, allowing for efficient calculations also for large molecular complexes. We have included the solvent effects by integrating the four-component relativistic density-functional theory program `ReSpect` [77] with the standalone library `PCMSolver` [78]. The formalism is general and although results have been presented only for the IEF-PCM model, the implementation is also applicable for the conductor-like screening model (COSMO).

Our results show that the importance of direct solvent effects to EPR parameters and pNMR shifts as described by the PCM is difficult to predict *a priori*, even though they are in many cases significant, amounting up to 25% of the gas-phase value, as demonstrated for the selected Ru and Os complexes. In other cases, such as the $[\mathrm{MEX}_n]^q$ d^1 complexes, there is hardly any noticeable direct solvent effect. The results presented in this contribution demonstrate the need to explore the relevance of solvent effects when computing EPR and pNMR parameters. The PCM provides a cost-effective strategy to carry out such an analysis and to possibly rule out whether consideration of solvent effects is mandatory or not. For pNMR chemical shifts, we found solvent effects to be sizeable, mandating their inclusion in precise calculations and/or reliable predictions and analysis. In addition, we observed an important role of van der Waals atomic radii employed in the construction of solvent-accessible surfaces, where results obtained by means of the UFF radii are notably outperformed by those using the radii derived from Allinger's MM3 model.

A detailed comparison with experiment is still difficult. One reason for this is our restriction to direct solvation effects. However, many experimental EPR studies are

conducted in solid matrices of the solute embedded in the solvent. It is not clear whether PCM would in this case be able to accurately model such medium effects. We also note that for charged metal complexes, the solvent molecules may directly coordinate with the complex, giving rise to changes in the molecular properties that arise from strong interactions with the electron density of the solute, which cannot be described by a dielectric continuum model alone. In this case, supermolecular complexes embedded in a dielectric continuum may be a good model to account for such effects.

In view of the fact that zero-point vibrational corrections have been shown to be important for hyperfine coupling constants, [122, 123] it can be expected that also geometry relaxation due to solvation can be significant to the EPR and temperature-dependent pNMR studies. The extension of the PCM model to geometry optimizations at the four-component level of theory is in progress in our group.

Acknowledgments

This work was supported by the Research Council of Norway (RCN) through a Center of Excellence (CoE) Grant and project grants (Grant No. 179568, 214095). The computational resources for this project have been provided by the NOTUR high performance computing program (Grant No. NN4654K). L.F. also acknowledges financial support by the Tromsø Research Foundation (SURFINT grant). P.H. acknowledges support from the Berlin DFG excellence cluster on Unifying Concepts in Catalysis (UniCat) and DFG project KA1187/13-1.

References

[1] J. E. Harriman, *Theoretical Foundations of Electron Spin Resonance*, Academic Press, New York, 1978.
[2] F. E. Mabbs and D. Collison, *Studies in Inorganic Chemistry*, Elsevier, 1992, vol. 16.
[3] *Calculation of NMR and EPR Parameters*, ed. M. Kaupp, M. Bühl and V. G. Malkin, Wiley-VCH Verlag GmbH & Co. KGaA, 2004.
[4] G. Hanson and L. Berliner, *Metals in biology: Applications of high resolution EPR to metalloenzymes*, Springer, 2010, vol. 29.
[5] F. Neese, J. M. Zaleski, K. L. Zaleski and E. I. Solomon, *J. Am. Chem. Soc.*, 2000, **122**, 11703.
[6] G. Schreckenbach and T. Ziegler, *J. Phys. Chem. A*, 1997, **101**, 3388.
[7] O. L. Malkina, J. Vaara, B. Schimmelpfennig, M. Munzarova, V. G. Malkin and M. Kaupp, *J. Am. Chem. Soc.*, 2000, **122**, 9206.
[8] F. Neese, *J. Chem. Phys.*, 2001, **115**, 11080.
[9] S. Patchkovskii and T. Ziegler, *J. Phys. Chem. A*, 2001, **105**, 5490–5497.
[10] F. Neese, *J. Chem. Phys.*, 2003, **118**, 3939.
[11] A. V. Arbuznikov, J. Vaara and M. Kaupp, *J. Chem. Phys.*, 2004, **120**, 2127–39.
[12] Z. Rinkevicius, L. Telyatnyk, O. Vahtras and H. Agren, *J. Chem. Phys.*, 2004, **121**, 7614–23.
[13] Z. Rinkevicius, K. J. de Almeida and O. Vahtras, *J. Chem. Phys.*, 2008, **129**, 064109.
[14] Z. Rinkevicius, K. J. de Almeida, C. I. Oprea, O. Vahtras, H. Å gren and K. Ruud, *J. Chem. Theory Comput.*, 2008, **4**, 1810–1828.
[15] L. F. Chibotaru and L. Ungur, *J. Chem. Phys.*, 2012, **137**, 064112.
[16] H. Bolvin, *ChemPhysChem*, 2006, **7**, 1575–1589.
[17] S. Vancoillie, P.-Å. Malmqvist and K. Pierloot, *ChemPhysChem*, 2007, **8**, 1803–1815.

[18] F. Gendron, B. Pritchard, H. Bolvin and J. Autschbach, *Inorg. Chem.*, 2014, **53**, 8577–8592.
[19] K. Sharkas, B. Pritchard and J. Autschbach, *J. Chem. Theory Comput.*, 2015, **11**, 538–549.
[20] T. Yanai, Y. Kurashige, W. Mizukami, J. Chalupskỳ, T. N. Lan and M. Saitow, *Int. J. Quantum Chem.*, 2015, **115**, 283–299.
[21] T. N. Lan, Y. Kurashige and T. Yanai, *J. Chem. Theory Comput.*, 2014, **10**, 1953–1967.
[22] S. Patchkovskii and T. Ziegler, *J. Chem. Phys.*, 1999, **111**, 5730.
[23] P. Hrobarik, M. Repisky, S. Komorovsky, V. Hrobarikova and M. Kaupp, *Theor. Chem. Acc.*, 2011, **129**, 715–725.
[24] S. Gohr, P. Hrobarik, M. Repisky, S. Komorovsky, K. Ruud and M. Kaupp, *J. Phys. Chem. A*, 2015, **119**, 12892–12905.
[25] E. Van Lenthe, P. E. Wormer and A. Van Der Avoird, *J. Chem. Phys.*, **107**, 2488–2498.
[26] E. van Lenthe, A. Van Der Avoird and P. E. Wormer, *J. Chem. Phys.*, 1998, **108**, 4783–4796.
[27] K. M. Neyman, D. I. Ganyushin, A. V. Matveev and V. A. Nasluzov, *J. Phys. Chem. A*, 2002, **106**, 5022–5030.
[28] I. Malkin, O. L. Malkina, V. G. Malkin and M. Kaupp, *Chem. Phys. Lett.*, 2004, **396**, 268–276.
[29] I. Malkin, O. L. Malkina, V. G. Malkin and M. Kaupp, *J. Chem. Phys.*, 2005, **123**, 244103.
[30] B. Sandhoefer and F. Neese, *J. Chem. Phys.*, 2012, **137**, 094102.
[31] P. Verma and J. Autschbach, *J. Chem. Theory Comput.*, 2013, **9**, 1932–1948.
[32] P. Verma and J. Autschbach, *J. Chem. Theory Comput.*, 2013, **9**, 1052–1067.
[33] R. Arratia-Perez and D. A. Case, *J. Chem. Phys.*, 1983, **79**, 4939–4949.
[34] H. Quiney, *Chem. Phys. Lett.*, 2002, **353**, 253–258.
[35] M. Repisky, S. Komorovsky, E. Malkin, O. L. Malkina and V. G. Malkin, *Chem. Phys. Lett.*, 2010, **488**, 94–97.
[36] E. Malkin, M. Repisky, S. Komorovsky, P. Mach, O. L. Malkina and V. G. Malkin, *J. Chem. Phys.*, 2011, **134**, 044111.
[37] M. S. Vad, M. N. Pedersen, A. Nørager and H. J. A. Jensen, *J. Chem. Phys.*, 2013, **138**, 214106.
[38] S. Moon and S. Patchkovskii, *Calculation of NMR and EPR Parameters. Theory and Applications*, Wiley-VCH, Weinheim, 2004, ch. 20.
[39] W. Van Den Heuvel and A. Soncini, *Phys. Rev. Lett.*, 2012, **109**, 073001.
[40] W. Van Den Heuvel and A. Soncini, *J. Chem. Phys.*, 2013, **138**, 054113.
[41] F. Gendron, K. Sharkas and J. Autschbach, *J. Phys. Chem. Lett.*, 2015, **6**, 2183–2188.
[42] T. O. Pennanen and J. Vaara, *J. Chem. Phys.*, 2005, **123**, 174102.
[43] P. Hrobarik, R. Reviakine, A. V. Arbuznikov, O. L. Malkina, V. G. Malkin, F. H. Köhler and M. Kaupp, *J. Chem. Phys.*, 2007, **126**, 024107.
[44] J. Autschbach, S. Patchkovskii and B. Pritchard, *J. Chem. Theory Comput.*, 2011, **7**, 2175–2188.
[45] S. Komorovsky, M. Repisky, K. Ruud, O. L. Malkina and V. G. Malkin, *J. Phys. Chem. A*, 2013, **117**, 14209.
[46] J. Vaara, S. A. Rouf and J. Mareš, *J. Chem. Theory Comput.*, 2015, **11**, 4840–4849.
[47] S. A. Rouf, J. Mareš and J. Vaara, *J. Chem. Theory Comput.*, 2015, **11**, 1683–1691.
[48] C. Reichardt and T. Welton, *Solvents and Solvent Effects in Organic Chemistry*, Wiley-VCH Verlag GmbH & Co. KGaA, Weinheim, 2010.
[49] B. Mennucci, J. Martínez and J. Tomasi, *J. Phys. Chem. A*, 2001, **105**, 7287–7296.
[50] I. Ciofini, *Calculation of NMR and EPR Parameters. Theory and Applications*, Wiley-VCH Verlag GmbH & Co. KGaA, Weinheim, 2004, pp. 191–208.
[51] J. Sadlej and M. Pecul, in *Computational Modelling of the Solvent–Solute Effect on NMR Molecular Parameters by a Polarizable Continuum Model*, ed. B. Mennucci and R. Cammi, John Wiley & Sons, Ltd, 2007, pp. 125–145.

[52] V. Barone, P. Cimino and M. Pavone, *Continuum Solvation Models in Chemical Physics*, John Wiley & Sons, Ltd, Chichester, 2007, p. 145.
[53] E. Pauwels, T. Verstraelen, H. De Cooman, V. Van Speybroeck and M. Waroquier, *J. Phys. Chem. B*, 2008, **112**, 7618–7630.
[54] H. M. Senn and W. Thiel, *Angew. Chem. Int. Edit.*, 2009, **48**, 1198–1229.
[55] J. Tomasi, B. Mennucci and R. Cammi, *Chem. Rev.*, 2005, **105**, 2999–3094.
[56] S. Sinnecker and F. Neese, *J. Comput. Chem.*, 2006, **27**, 1463–1475.
[57] C. Houriez, N. Ferré, M. Masella and D. Siri, *J. Chem. Phys.*, 2008, **128**, 244504.
[58] E. Pauwels, R. Declerck, T. Verstraelen, B. De Sterck, C. W. Kay, V. Van Speybroeck and M. Waroquier, *J. Phys. Chem. B*, 2010, **114**, 16655–16665.
[59] Z. Rinkevicius, N. A. Murugan, J. Kongsted, K. Aidas, A. H. Steindal and H. Ågren, *J. Phys. Chem. B*, 2011, **115**, 4350–4358.
[60] Z. Rinkevicius, N. A. Murugan, J. Kongsted, B. Frecus, A. H. Steindal and H. Ågren, *J. Chem. Theory Comput.*, 2011, **7**, 3261–3271.
[61] F. Lipparini, C. Cappelli and V. Barone, *J. Chem. Phys.*, 2013, **138**, 234108.
[62] *Continuum Solvation Models in Chemical Physics*, ed. B. Mennucci and R. Cammi, John Wiley & Sons, Ltd, Chichester, 2007.
[63] C. Amovilli and B. Mennucci, *J. Phys. Chem. B*, 1997, **101**, 1051–1057.
[64] V. Weijo, B. Mennucci and L. Frediani, *J. Chem. Theory Comput.*, 2010, **6**, 3358–3364.
[65] C. Adamo, M. Heitzmann, F. Meilleur, N. Rega, G. Scalmani, A. Grand, J. Cadet and V. Barone, *J. Am. Chem. Soc.*, 2001, **123**, 7113–7117.
[66] M. Kaupp, C. Remenyi, J. Vaara, O. L. Malkina and V. G. Malkin, *J. Am. Chem. Soc.*, 2002, **124**, 2709–2722.
[67] J. Novotny, M. Sojka, S. Komorovsky, M. Necas and R. Marek, *J. Am. Chem. Soc.*, 2016, doi:10.1021/jacs.6b02749.
[68] J. Autschbach and T. Ziegler, *J. Am. Chem. Soc.*, 2001, **123**, 3341–9.
[69] J. Autschbach and B. Le Guennic, *J. Am. Chem. Soc.*, 2003, **125**, 13585–93.
[70] A. Antušek, M. Pecul and J. Sadlej, *Chem. Phys. Lett.*, 2006, **427**, 281–288.
[71] J. Autschbach and M. Sterzel, *J. Am. Chem. Soc.*, 2007, **129**, 11093–11099.
[72] M. Olejniczak and M. Pecul, *Chemphyschem*, 2009, **10**, 1247–1259.
[73] S. Zheng and J. Autschbach, *Chem. Eur. J.*, 2011, **17**, 161–173.
[74] J. Vicha, M. Patzschke and R. Marek, *Phys. Chem. Chem. Phys.*, 2013, **15**, 7740–7754.
[75] J. Vicha, J. Novotny, M. Straka, M. Repisky, K. Ruud, S. Komorovsky and R. Marek, *Phys. Chem. Chem. Phys.*, 2015, **17**, 24944–24955.
[76] R. Di Remigio, R. Bast, L. Frediani and T. Saue, *J. Phys. Chem. A*, 2015, **119**, 5061–5077.
[77] `ReSpect`, version 3.5.0 (2016) – Relativistic Spectroscopy DFT program of authors Repisky, M.; Komorovsky, S.; Malkin, V. G.; Malkina, O. L.; Kaupp, M.; Ruud, K., with contributions from Bast, R.; Ekström, U.; Kadek, M.; Knecht, S.; Konecny, L.; Malkin, E.; Malkin-Ondik, I.; Remigio, R. Di (see http://www.respectprogram.org).
[78] `PCMSolver`, an Application Programming Interface for the Polarizable Continuum Model electrostatic problem, written by R. Di Remigio, L. Frediani and K. Mozgawa, (see http://pcmsolver.readthedocs.org/).
[79] J. Tomasi and M. Persico, *Chem. Rev.*, 1994, **94**, 2027–2094.
[80] J. D. Jackson, *Classical Electrodynamics*, John Wiley & Sons, New York, 1998.
[81] J. Vanderlinde, *Classical Electromagnetic Theory*, Springer, Dordrecht, 2005.
[82] E. Cancès and B. Mennucci, *J. Math. Chem.*, 1998, **23**, 309.
[83] W. Hackbusch, *Integral Equations – Theory and Numerical Treatment*, Birkhaüser, Basel, 1995.
[84] G. C. Hsiao and W. L. Wendland, *Boundary Integral Equations*, Springer, Berlin, 2008, vol. 164.
[85] L. Frediani, R. Cammi, S. Corni and J. Tomasi, *J. Chem. Phys.*, 2004, **120**, 3893–3907.
[86] R. Di Remigio, K. Mozgawa, H. Cao, V. Weijo and L. Frediani, 2016, (submitted).
[87] A. Delgado, S. Corni and G. Goldoni, *J. Chem. Phys.*, 2013, **139**, 024105.

[88] A. Ern and J.-L. Guermond, *Theory and practice of finite elements*, Springer, New York, 2004.
[89] E. Silla, J. L. Pascual-Ahuir, J. Tomasi and R. Bonaccorsi, *J. Comp. Chem.*, 1987, **8**, 778–787.
[90] C. S. Pomelli, *Continuum Solvation Models in Chemical Physics*, John Wiley & Sons, Ltd, Chichester, 2007, pp. 49–63.
[91] A. Klamt and G. Schüürmann, *J. Chem. Soc., Perkin Trans. 2*, 1993, 799–805.
[92] C. C. Pye and T. Ziegler, *Theor. Chem. Acc.*, 1999, **101**, 396–408.
[93] M. Cossi, N. Rega, G. Scalmani and V. Barone, *J. Comput. Chem.*, 2003, **24**, 669–81.
[94] T. Helgaker, P. Jørgensen and J. Olsen, *Molecular Electronic-Structure Theory*, John Wiley & Sons, Ltd, Chichester, 2000.
[95] K. G. Dyall and K. Fægri, Jr., *An Introduction to Relativistic Quantum Chemistry*, Oxford University Press, New York, 2007.
[96] M. Reiher and A. Wolf, *Relativistic Quantum Chemistry*, Wiley-VCH Verlag GmbH & Co. KGaA, Weinheim, 2009.
[97] P. Cherry, S. Komorovsky, V. G. Malkin and O. L. Malkina, *Mol. Phys.*, 2016, doi:10.1080/00268976.2016.1191688.
[98] V. A. Dzuba, V. V. Flambaum and O. P. Sushkov, *J. Phys. B: At. Mol. Phys.*, 1984, **17**, 1953–1968.
[99] L. M. Sandratskii, *Adv. Phys.*, 1998, **47**, 91–160.
[100] C. van Wüllen, *J. Comput. Chem.*, 2002, **23**, 779–785.
[101] G. Scalmani and M. J. Frisch, *J. Chem. Theory Comp.*, 2012, **8**, 2193–2196.
[102] H. M. McConnell and D. B. Chesnut, *J. Chem. Phys.*, 1958, **28**, 107–117.
[103] H. M. McConnell and R. E. Robertson, *J. Chem. Phys.*, 1958, **29**, 1361–1365.
[104] R. J. Kurland and B. R. McGarvey, *J. Magn. Reson.*, 1970, **2**, 286–301.
[105] J. P. Perdew, K. Burke and M. Ernzerhof, *Phys. Rev. Lett.*, 1996, **77**, 3865–3868.
[106] C. Adamo and V. Barone, *J. Chem. Phys.*, 1999, **110**, 6158–6169.
[107] S. Grimme, J. Antony, S. Ehrlich and H. Krieg, *J. Chem. Phys.*, 2010, **132**, 154104.
[108] S. Grimme, S. Ehrlich and L. Goerigk, *J. Comput. Chem.*, 2011, **32**, 1456–1465.
[109] D. Andrae, U. Häuß ermann, M. Dolg, H. Stoll and H. Preuß, *Theor. Chim. Acta*, 1990, **77**, 123–141.
[110] F. Weigend and R. Ahlrichs, *Phys. Chem. Chem. Phys.*, 2005, **7**, 3297–3305.
[111] L. Visscher and K. G. Dyall, *At. Data Nucl. Data Tables*, 1997, **67**, 207–224.
[112] F. Jensen, *J. Chem. Theory Comput.*, 2006, 1360–1369.
[113] K. G. Dyall, *Theor. Chem. Acc.*, 2006, **117**, 483–489.
[114] K. G. Dyall, *Theor. Chem. Acc.*, 2004, **112**, 403–409.
[115] K. G. Dyall and A. S. P. Gomes, *Theor. Chem. Acc.*, 2010, **125**, 97–100.
[116] N. L. Allinger, X. Zhou and J. Bergsma, *Journal of Molecular Structure: THEOCHEM*, 1994, **312**, 69–83.
[117] S. Frantz, B. Sarkar, M. Sieger, W. Kaim, F. Roncaroli, J. A. Olabe and S. Záliš, *Eur. J. Inorg. Chem.*, 2004, **2004**, 2902–2907.
[118] W. M. Ames and S. C. Larsen, *J. Phys. Chem. A*, 2009, **113**, 4305–4312.
[119] K. J. de Almeida, T. C. Ramalho, Z. Rinkevicius, O. Vahtras, H. Ågren and A. Cesar, *J. Phys. Chem. A*, 2011, **115**, 1331–1339.
[120] C. Finazzo, C. Calle, S. Stoll, S. Van Doorslaer and A. Schweiger, *Phys. Chem. Chem. Phys.*, 2006, **8**, 1942–1953.
[121] A. K. Rappe, C. J. Casewit, K. S. Colwell, W. A. Goddard and W. M. Skiff, *J. Am. Chem. Soc.*, 1992, **114**, 10024–10035.
[122] X. Chen, Z. Rinkevicius, Z. Cao, K. Ruud and H. Ågren, *Phys. Chem. Chem. Phys.*, 2010, **13**, 696–707.
[123] X. Chen, Z. Rinkevicius, K. Ruud and H. Ågren, *J. Chem. Phys.*, 2013, **138**, 054310.
[124] A. Voigt, U. Abram and R. Kirmse, *Inorg. Chem. Commun.*, 1998, **1**, 141–142.
[125] G. M. Lack and J. F. Gibson, *J. Mol. Struct.*, 1978, **46**, 299–306.
[126] M. Wanner, T. Scheiring, W. Kaim, L. D. Slep, L. M. Baraldo, J. A. Olabe, S. Záliš and

E. J. Baerends, *Inorg. Chem.*, 2001, **40**, 5704–5707.
[127] P. Singh, B. Sarkar, M. Sieger, M. Niemeyer, J. Fiedler, S. Záliš and W. Kaim, *Inorg. Chem.*, 2006, **45**, 4602–4609.
[128] B. Delley, *Mol. Simul.*, 2006, **32**, 117–123.

Table 1. Effect of a polarizable continuum solvent model (IEF-PCM) on computed principal components of the electronic Δg tensor [ppt] and of the metal HFC tensor [MHz] in selected Re^{VI} complexes.[a]

Complex	Method	Solvent	$\Delta g_{\parallel}$	$\Delta g_{\perp}$	$\Delta g_{\rm iso}$	$A_{\parallel}^{\rm M}$	$A_{\perp}^{\rm M}$	$A_{\rm iso}^{\rm M}$
$[^{187}ReNF_4]^-$	PBE0	in vacuo	-324	-115	-185	-2792	-1355	-1834
		IEF-PCM[b]	-333	-112	-186	-2831	-1379	-1863
	PBE0-40	in vacuo	-349	-120	-196	-3099	-1643	-2128
		IEF-PCM[b]	-358	-118	-198	-3147	-1675	-2166
	Expt.[c,e]	**CH_3CN**	**-353**	**-132**	**-206**	**-3079**	**-1637**	**-2118**
$[^{187}ReNCl_4]^-$	PBE0	in vacuo	-64	-70	-68	-2007	-872	-1250
		IEF-PCM[b]	-63	-69	-67	-2011	-871	-1251
	PBE0-40	in vacuo	-92	-76	-81	-2285	-1118	-1507
		IEF-PCM[b]	-92	-75	-81	-2290	-1119	-1510
	Expt.[d,e]	**CH_3CN**	**-93**	**-68**	**-77**	**-2308**	**-1145**	**-1533**

[a] This work. All calculations were done at 4c-DKS/Dyall(vTZ)/upcJ-2 level with or without the IEF-PCM solvation model, employing the traditional PBE0 hybrid functional or PBE0-40 with a customized (40%) admixture of Hartree–Fock exchange.
[b] The value of the static permittivity $\varepsilon_{\rm r} = 37.5$ used for CH_3CN as solvent.
[c] Expt. value taken from Ref. [124].
[d] Expt. value taken from Ref. [125].
[e] Experimental errors: $\Delta g_i \pm 3$ ppt, $A_i^{\rm M} = \pm 15$ MHz; estimated from linewidth analysis.

Table 2. Effect of a polarizable continuum solvent model (IEF-PCM) on computed principal components of the electronic Δg tensor [ppt] in selected Ru and Os nitrosyl complexes.[a]

Complex	Method	Solvent	Δg_{11}	Δg_{22}	Δg_{33}	$\Delta g_{\rm iso}$
$[Ru(CN)_5(NO)]^{3-}$	PBE0	in vacuo	-161	-22	-5	-63
		IEF-PCM[b]	-143	-16	-7	-55
	PBE0-40	in vacuo	-180	-27	-4	-70
		IEF-PCM[b]	-152	-17	-8	-59
	Expt.[c]	**CH_3CN**	**-132**	**0**	**2**	**-44**
$[Os(CN)_5(NO)]^{3-}$	PBE0	in vacuo	-411	-87	-31	-177
		IEF-PCM[b]	-358	-69	-33	-153
	PBE0-40	in vacuo	-488	-98	-32	-206
		IEF-PCM[b]	-381	-74	-30	-162
	Expt.[c]	**CH_3CN**	**-368**	**-71**	**-43**	**-161**
cis-$[RuCl(bpy)_2(NO)]^{+}$	PBE0	in vacuo	-113	-22	17	-39
		IEF-PCM[b]	-122	-24	17	-43
	PBE0-40	in vacuo	-131	-26	17	-47
		IEF-PCM[b]	-138	-29	18	-50
	Expt.[d]	**CH_3CN**	**-121**	**-10**	**27**	**-35**
cis-$[OsCl(bpy)_2(NO)]^{+}$	PBE0	in vacuo	-268	-71	9	-110
		IEF-PCM[b]	-332	-90	8	-138
	PBE0-40	in vacuo	-332	-89	13	-136
		IEF-PCM[b]	-401	-113	22	-164
	Expt.[e,f]	**CH_3CN**	**-382**	**-112**	**-22**	**-172**

[a] This work. All calculations were done at 4c-DKS/Dyall(vTZ)/upcJ-2 level with or without the IEF-PCM solvation model, employing the traditional PBE0 hybrid functional or PBE0-40 with a customized (40%) admixture of Hartree–Fock exchange.
[b] The value of the static permittivity $\varepsilon_{\rm r} = 37.5$ used for CH_3CN as solvent.
[c] Expt. value taken from Ref. [126].
[d] Expt. value taken from Ref. [117].
[e] Expt. value taken from Ref. [127].
[f] Experimental errors: $\Delta g_i \pm 10$ ppt; estimated from linewidth analysis.

Table 3. Effect of various solvent models on computed ^{1}H and ^{13}C temperature-dependent contribution to pNMR shifts [ppm] in selected Ru(III) complexes.[a]

Complex	Nucleus	Solvation Model				Expt.[e]
		in vacuo[a]	IEF-PCM[a,b]	IEF-PCM[a,c]	COSMO[d]	
$[RuCl_4(DMSO)(4\text{-Me-py})]^-$	H2	-6.7	-11.6	-14.1	-14.8	-14.0
	H3	-8.9	-9.5	-10.3	-9.7	-9.4
	H_{Me}	-8.5	-6.6	-6.2	-6.1	-6.0
	H_{DMSO}	-12.4	-14.3	-15.6	-17.1	-15.5
	C2	-73	-70	-74	-75	-72
	C3	-7	-19	-23	-28	-25
	C4	-49	-33	-30	-28	-27
	C_{Me}	11	4	1	2	0
	C_{DMSO}	-180	-162	-150	-163	-156
	MAE[f]	**9.9**	**3.2**	**1.8**	**2.1**	
$[RuCl_4(DMSO)(4\text{-CN-py})]^-$	H2	-1.8	-7.3	-10.8	-10.8	-11.9
	H3	-9.7	-9.8	-10.3	-9.9	-8.5
	H_{DMSO}	-12.4	-14.2	-15.5	-16.9	-15.7
	C2	-84	-81	-84	-86	-78
	C3	13	-4	-12	-15	-17
	C4	-78	-52	-42	-42	-34
	C_{CN}	52	29	20	21	11
	C_{DMSO}	-175	-159	-148	-160	-146
	MAE[f]	**20.6**	**9.0**	**3.8**	**5.7**	

[a]This work. Data calculated at 4c-DKS/Dyall(vTZ)/upcJ-2 level of theory with the PBE0 hybrid functional.
[b]IEF-PCM using a solvent-accessible surface with UFF radii [121]: 1.4430 Å for H, 1.4815 Å for Ru, 1.9255 Å for C, 2.0175 Å for S, 1.75 Å for O, 1.9735 Å for Cl and 1.83 Å for N. All radii were multiplied by a factor of 1.2. The value of the static permittivity for DMF ($\varepsilon_r = 37.0$) was used.
[c]IEF-PCM using a solvent-accessible surface with radii from Allinger's MM3 model [116] (see Section 3 for more details). The value of the static permittivity for DMF ($\varepsilon_r = 37.0$) was used.
[d]Calculations at the ZORA-SO/PBE0/TZ2P level of theory with the COSMO solvation model. [67] A Delley surface [128] with radii from Allinger's MM3 model was used [116] (see Section 3 for more details). The value of the static permittivity for DMF ($\varepsilon_r = 37.0$) was used.
[e]Experimental data measured in dimethylformamide and taken from Ref. [67]
[f]Mean absolute error between calculated and experimental data. [f]Mean absolute error between calculated and experimental data.

Figure 1. Schematic structures of the investigated transition-metal complexes. Atom numbering in ligands of two Ru(III) complexes employed in pNMR calculations is given as well.

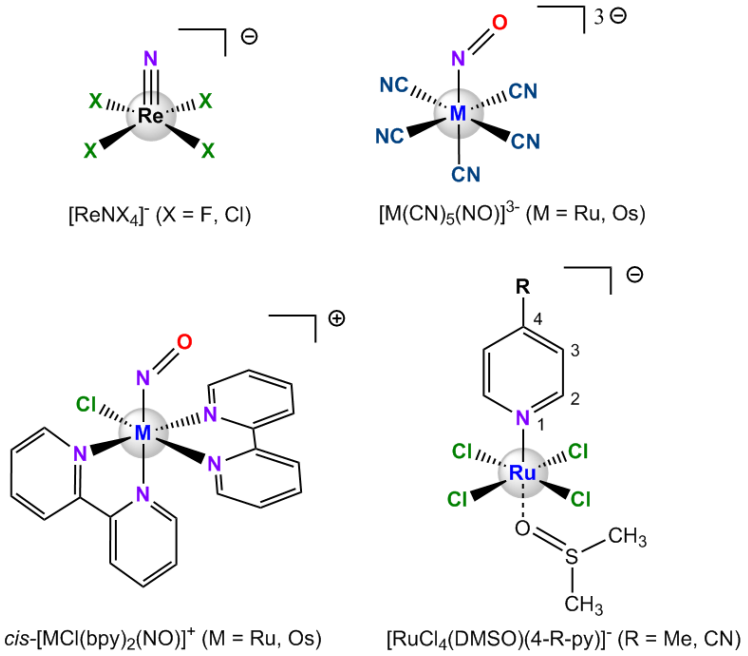

Figure 2. (a) Visualization of the electronic $\Delta\mathbf{g}$-tensor and its principal axes in $[Os(CN)_5(CN)]^{3-}$. (b) The dependency of Δg_{ii} values on solvent polarity.

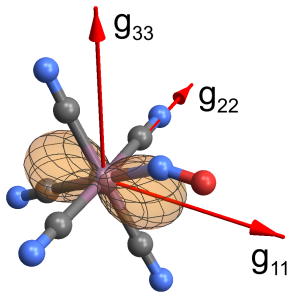

(a)

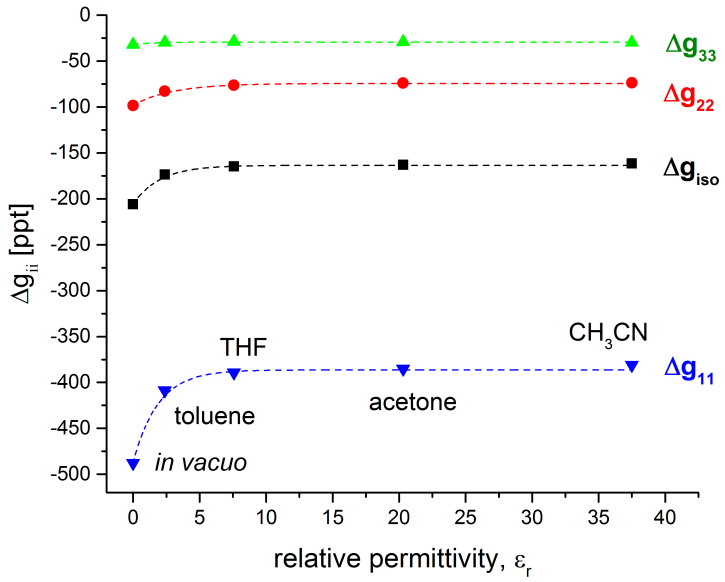

(b)

SUPPLEMENTARY INFORMATION

Four-Component Relativistic Density Functional Theory with the Polarizable Continuum Model: Application to EPR Parameters and Paramagnetic NMR Shifts

Roberto Di Remigio[a], Michal Repisky[a], Stanislav Komorovsky[a], Peter Hrobarik[b], Luca Frediani[a], and Kenneth Ruud[a]

[a]Centre for Theoretical and Computational Chemistry, Department of Chemistry, University of Tromsø - The Arctic University of Norway, N-9037 Tromsø, Norway
[b]Institut für Chemie, Technische Universität Berlin, Straße des 17. Juni 135, D-10623 Berlin, Germany

ARTICLE HISTORY
Compiled February 24, 2017

Table 1. Comparison of computed principal components of $\boldsymbol{g}$-tensor in selected Ru(III) complexes.

Complex	Solvation Model	Principal components			
		g_{11}	g_{22}	g_{33}	g_{iso}
$[RuCl_4(DMSO)(4\text{-Me-py})]^-$	in vacuo[a]	-101	286	320	168
	IEF-PCM[a,b]	-202	344	380	174
$[RuCl_4(DMSO)(4\text{-CN-py})]^-$	in vacuo[a]	-84	266	321	167
	IEF-PCM[a,b]	-177	328	372	174

[a]This work. Data calculated at 4c-DKS/Dyall(vTZ)/upcJ-2 level of theory with the PBE0 hybrid functional.
[b]Integral Equation Formalism (IEF)-Polarizable Continuum Model (PCM) using a solvent-accessible surface with radii from Allinger's MM3 model [1] (see Section 3 for more details). The value of the static permittivity for dimethylformamide (DMF) ($\varepsilon_{\mathrm{r}} = 37.0$) was used.

Table 2. Comparison of computed ^{1}H and ^{13}C principal components of $\boldsymbol{A}$-tensor [MHz], and contact and pseudocontact contributions[a] to pNMR shifts [ppm] in selected Ru(III) complexes.

Complex	Nucleus	Solvation Model	Principal components[b]					
			A_{11}	A_{22}	A_{33}	A_{iso}	δ^{fc}	δ^{pc}
$[RuCl_4(DMSO)(4\text{-Me-py})]^-$	H2	in vacuo[c]	-2.70	0.32	2.12	-0.09	-2.5	-4.2
		IEF-PCM[c,d]	-2.96	0.16	1.93	-0.29	-8.5	-5.7
	H3	in vacuo[c]	-0.75	-0.52	0.51	-0.26	-7.4	-1.4
		IEF-PCM[c,d]	-0.78	-0.55	0.48	-0.29	-8.3	-1.9
	H_{Me}	in vacuo[c]	-0.49	-0.45	0.14	-0.27	-7.8	-0.7
		IEF-PCM[c,d]	-0.41	-0.34	0.22	-0.18	-5.2	-1.0
	H_{DMSO}	in vacuo[c]	-1.56	-0.97	1.50	-0.34	-10.0	-2.4
		IEF-PCM[c,d]	-1.62	-1.03	1.41	-0.41	-12.1	-3.5
	C2	in vacuo[c]	-1.55	-0.72	0.59	-0.56	-64.8	-8.5
		IEF-PCM[c,d]	-1.33	-0.81	0.50	-0.55	-63.6	-10.6
	C3	in vacuo[c]	-0.33	0.03	0.15	-0.05	-5.8	-1.4
		IEF-PCM[c,d]	-0.41	-0.18	0.05	-0.18	-20.9	-2.3
	C4	in vacuo[c]	-1.12	-0.21	0.19	-0.38	-44.3	-4.4
		IEF-PCM[c,d]	-0.70	-0.17	0.22	-0.22	-25.3	-4.4
	C_{Me}	in vacuo[c]	0.02	0.04	0.25	0.10	12.0	-1.0
		IEF-PCM[c,d]	-0.06	-0.04	0.17	0.02	2.8	-1.5
	C_{DMSO}	in vacuo[c]	-1.89	-1.82	-0.82	-1.51	-175.4	-4.6
		IEF-PCM[c,d]	-1.64	-1.47	-0.59	-1.24	-143.7	-6.1
$[RuCl_4(DMSO)(4\text{-CN-py})]^-$	H2	in vacuo[c]	-2.58	0.51	2.31	0.08	2.3	-4.1
		IEF-PCM[c,d]	-2.89	0.30	2.04	-0.18	-5.3	-5.5
	H3	in vacuo[c]	-0.78	-0.55	0.46	-0.29	-8.4	-1.3
		IEF-PCM[c,d]	-0.79	-0.55	0.47	-0.29	-8.5	-1.8
	H_{DMSO}	in vacuo[c]	-1.57	-0.97	1.50	-0.35	-10.1	-2.3
		IEF-PCM[c,d]	-1.63	-1.04	1.41	-0.42	-12.2	-3.3
	C2	in vacuo[c]	-1.91	-0.67	0.65	-0.64	-74.3	-9.3
		IEF-PCM[c,d]	-1.57	-0.82	0.51	-0.63	-72.8	-10.9
	C3	in vacuo[c]	-0.23	0.28	0.30	0.12	13.9	-0.8
		IEF-PCM[c,d]	-0.36	-0.01	0.11	-0.09	-10.3	-1.7
	C4	in vacuo[c]	-1.77	-0.24	0.14	-0.62	-72.1	-5.9
		IEF-PCM[c,d]	-0.95	-0.19	0.20	-0.31	-36.5	-5.0
	C_{CN}	in vacuo[c]	0.37	0.47	0.53	0.45	52.5	0.0
		IEF-PCM[c,d]	0.07	0.19	0.27	0.18	20.7	-0.8
	C_{DMSO}	in vacuo[c]	-1.86	-1.78	-0.79	-1.47	-171.1	-4.3
		IEF-PCM[c,d]	-1.62	-1.47	-0.57	-1.22	-141.9	-5.7

[a] For the decomposition of the temperature-dependent contribution to the isotropic pNMR shift in the four-component framework see Ref. [2].
[b] Principal components were calculated from symmetric diagonalization of the $\boldsymbol{A}$-tensor $[1/2(A + A^T)]$.
[c] This work. Data calculated at 4c-DKS/Dyall(vTZ)/upcJ-2 level of theory with the PBE0 hybrid functional.
[d] IEF-PCM using a solvent-accessible surface with radii from Allinger's MM3 model [1] (see Section 3 for more details). The value of the static permittivity for DMF ($\varepsilon_r = 37.0$) was used.

References

[1] N. L. Allinger, X. Zhou and J. Bergsma, *Journal of Molecular Structure: THEOCHEM*, 1994, **312**, 69–83.

[2] S. Komorovsky, M. Repisky, K. Ruud, O. L. Malkina and V. G. Malkin, *J. Phys. Chem. A*, 2013, **117**, 14209.